Fine structure transitions with spectral features in Fe V and Fe VI

Sultana N. Nahar

The Ohio State University, Department of Astronomy, Columbus, 43210, OH, USA

ARTICLE INFO

ABSTRACT

An extensive set of E1 transitions with spectral features for Fe V obtained using relativistic Breit–Pauli R-matrix (BPRM) method is presented. The results correspond to a larger amount of atomic data and of higher accuracy in comparison to the earlier R-matrix results. We report 1,712,655 transitions among 4300 fine structure levels with $j \leq 10$, $2S + 1 = 5$, 3, 1, $L \leq 10$, of even and odd parities of n $\leq$ 10 and $l \leq 9$. The close coupling wavefunction expansion of Fe V includes ground and 18 excited levels of the core ion Fe VI. The theoretical spectroscopy of the fine structure levels for unique identifications was carried out using an algorithm based on quantum defect theory and angular algebra. The completeness of the calculated data sets is verified for all possible bound levels belonging to the relevant LS terms. The energies are in very good agreement with measured values within a few percent for most levels. Comparison of transition parameters and lifetimes also indicate general agreement with others. The present data processed for spectral features that show the detectability of Fe V is well within range of James Webb Space Telescope and other observatories.

The present results for Fe VI, obtained from relativistic atomic structure calculations in Breit–Pauli approximation using code SUPERSTRUCTURE, include allowed E1 and forbidden E2, M1, E3, M2 transitions, 506,512 in total among 1021 energy levels, bound and continuum. Calculations show much larger number of bound levels of configurations of $3s^2 3p^5 3d^4$ than those listed at NIST compilation table. The calculations included an optimized set of 9 configurations with orbitals going up to 4f. Comparison of energies, oscillator strengths, lifetimes with available values show good agreement although some large differences are also noted. In contrast to Fe V, the spectral features of Fe VI show three regions of strong lines in the soft-xray to ultraviolet wavelengths.

Contents

1. Introduction

Photo-excitation of ion X^{+Z}, where X is the ion of charge Z, may be expressed as

$$X^{+Z} + h\nu \rightleftharpoons X^{+Z*} \tag{1}$$

where $h\nu$ is the photon and $*$ indicates an excited state. The process can also lead to a doubly excited state. Then after the lifetime of the state, the ion decays to a lower excited or to its original ground state. This photo-absorption and emission introduces a discrete spectral line. Although several processes can contribute to a spectral line, astrophysical spectra are dominated largely by discrete lines of atomic radiative transitions and a set of large number of transition lines can provide an overall spectral features of the species. The present work reports calculation of extensive set of energies, transition parameters, lifetimes, spectroscopy of lines, and spectral features of two iron ions, Fe V and Fe VI.

Iron is the most abundant element, following H, He, C, N, O, and appear in various ionization stages in astronomical objects. Low ionization stages of iron ions have been seen in diffuse and planetary nebulae, e.g. [1,2]. Fe V spectra have been observed in young, hot DA white dwarf atmospheres by the International Ultraviolet Explorer (IUE) and the Extreme Ultraviolet Explorer (EUV E), e.g. [3–5]. With open d-orbital these ions have large number of energy levels, and hence corresponding large number of transition among them. The comprehensive models for astrophysical and laboratory applications, such as opacities [6,7], radiative forces [8–10], radiation transport in high-density fusion plasma, etc. require large data sets that are complete and accurate. However, lack of detailed and accurate calculations for the atomic parameters of these ions is due to the difficulty introduced by the large number of highly coupled states and resonances. The first systematic study of the iron ions using an ab initio R-matrix method with close coupling approximation was carried out under the Opacity Project (OP) [11] and the Iron Project (IP) [12]. Existing R-matrix codes, e.g. [13–15], were extended extensively [16–18] for large scale computations of accurate parameters for the atomic processes. The huge amount of atomic data computed under projects are available in three databases, TOPbase [19], TIPbase [20], and NORAD-Atomic-Data [21]. However, most of the calculations under the OP were carried out in non-relativistic LS coupling approximation. As need for fine structure transitions was realized, transitions in LS multiplets were converted to fine structure through algebraic transformations, e.g. [22].

Relativistic effects were included later in the codes for Breit–Pauli R-matrix method (BPRM) [18] and the first BPRM transitions reported were for Fe XXIV and Fe XXV in Nahar and Pradhan [23].

The present work reports large sets of energies, transition parameters, lifetimes for Fe V and Fe VI obtained in relativistic fine structure. Observed energies for Fe V and Fe VI measured by Sugar and Corliss [24] for a limited number of levels are available from NIST compilation table [25]. Lifetimes of a number of excited levels of both Fe V and Fe VI were measured using beam-foil technique by Dumont et al. [26]. This paper also reports the calculated lifetimes of Fe V and Fe VI using transitions obtained by Abbott [27]. These two ions were studied theoretically under the OP [11] and the IP [12] using the R-matrix method and close coupling approximation.

For Fe V, radiative transitions were calculated by Bautista [28], Nahar et al. [29,30], photoionization cross sections were obtained by Bautista [28], and electron-ion recombination of Fe V by Nahar and Bautista [31]. Transitions in Fe V were studied earlier using atomic structure calculation by Abbott [27], Fawcett [32] and more recently for 182 levels by Aggarwal et al. [33].

The earlier work on E1 transitions in fine structure for Fe V were obtained using the relativistic BPRM method by Nahar et al. [29,30]. However, later a bug was detected and corrected in one program called RECUPD of the BPRM package of codes in early 2007. The bug affected certain bound–bound transitions. The present work reports the repeated calculations for Fe V, but using a different wavefunction expansion and for a larger sets of energy levels and transitions and more accurate values.

For Fe VI, radiative transitions were calculated by Butler et al. [19,34], and electron impact excitation were studied by Chen and Pradhan [35,36]. This work reports allowed and forbidden transitions about the 80 fine structure levels belonging to configurations $3d^3$, $3d^24s$, and $3d^24p$, obtained using the Breit–Pauli version of the code SUPERSTRUCTURE [37]. The earlier work on Fe VI transitions is correspond to Garstang et al. [38]. NIST reports 159 forbidden transitions in Fe VI of type E2 and M1 calculated by Nussbaumer and Storey [39]. Objective of all these work is discuss and report excitation collision strengths for which forbidden E2, M1 transitions for Fe VI are needed. However, Chen and Pradhan [35,36] provide table of E1 transitions of 81 levels. Present Fe VI transitions have been obtained from atomic structure calculations in relativistic Breit–Pauli approximation using code SUPERSTRUCTURE [37,40,41]. The results are for fine structure transitions and includes both allowed E1 and forbidden transitions in

contrast to earlier results under the OP available only for dipole allowed transitions in LS coupling [19,34].

2. Theory

The two methodologies employed here for radiative transitions, Breit–Pauli R-matrix (BPRM) method [11,12] for Fe V and atomic structure calculations in Breit–Pauli approximation using program SUPERSTRUCTURE (SS) [37,41] for Fe VI, include relativistic fine structure effects. There are some differences between the two packages of codes. While BPRM codes can generate a much larger set of dipole allowed E1 transitions than SS, SS can compute both dipole allowed E1 and forbidden electric quadrupole (E2), electric octupole (E3), magnetic dipole (M1), magnetic quadrupole (M2) transitions. Calculations using BPRM codes [17,18] are *ab initio* since they do not use any model potential, SUPERSTRUCTURE [37,40,41] implements Thomas–Fermi–Dirac–Amaldi (TFDA) potential to represent the electron–electron interactions. The present results are related to both approaches since Fe VI wavefunctions created by SS were implemented as the core ion wavefunctions in the BPRM calculations for Fe V.

A brief outline of the methods is described below.

2.1. Relativistic Breit–Pauli approximation

In relativistic Breit–Pauli approximation, Schrodinger equation,

$$H_{\mathrm{BP}}\Psi = E\Psi. \tag{2}$$

is solved with the Hamiltonian (e.g. [41,42])

$$H_{\mathrm{BP}} = H_{N+1}^{NR} + H_{\mathrm{mass}} + H_{\mathrm{Dar}} + H_{\mathrm{so}}+$$

$$\frac{1}{2}\sum_{i \neq j}^{N}\{[g_{ij}(so+so') + g_{ij}(ss')] + g_{ij}(css') + g_{ij}(d) + g_{ij}(oo')\} \tag{3}$$

where H_{N+1}^{NR} is the non-relativistic Hamiltonian,

$$H_{N+1}^{\mathrm{NR}} = \sum_{i=1}^{N+1}\left\{-\nabla_i^2 - \frac{2Z}{r_i} + \sum_{j>i}^{N+1}\frac{2}{r_{ij}}\right\},. \tag{4}$$

N is the number of core ion electrons. The next three terms in H_{BP} are 1-body correction terms known as the mass correction, Darwin and spin–orbit interaction terms,

$$H_{\mathrm{mass}} = -\frac{\alpha^2}{4}\sum_i p_i^4, \quad H_{\mathrm{Dar}} = \frac{\alpha^2}{4}\sum_i \nabla^2\left(\frac{Z}{r_i}\right), \quad H_{so} = \frac{Ze^2\hbar^2}{2m^2c^2r^3}\sum_i \mathbf{l_i}\cdot\mathbf{s_i} \tag{5}$$

$\mathbf{p}_i$ is the electron momentum, $\mathbf{l}_i$ and $\mathbf{s}_i$ are orbital and spin angular momenta, and α is the fine structure constant. The rest terms in H_{BP} are 2-body terms of spin and orbit interactions. Program SS [41] includes contributions of the three 1-body terms, the 2-body Breit interaction term (the first two spin–orbit interaction terms within square brackets), and part of last three terms. However, BPRM codes [18] include the 1-body correction terms only.

Each relativistic correction term improves the accuracy of energy levels and hence transitions over the non-relativistic LS coupling energies and transitions. Hence, SS program improves accuracy by inclusion of the additional terms in comparison to BPRM method. However, accuracy can be enhanced faster with increment in configuration interaction than the correction terms. The R-matrix method incorporates much more configuration interaction than atomic structure calculations. Hence, R-matrix results are often more accurate than those of SS.

2.2. Wavefunctions and energies

BPRM method implements close coupling approximation (CC) for the wavefunction where the atomic system is described by an N-

electrons core ion is interacting with the (N+1)th electron. The total (e+ion) wave function, Ψ_E, in a symmetry $SL\pi J$ is expressed as (e.g. [42])

$$\Psi_E(e + ion) = A\sum_i \chi_i(ion)\theta_i + \sum_j c_j\Phi_j, \tag{6}$$

where χ_i is the core ion eigen function at the ground and various excited levels and the sum is over the number of core ion excitation considered for the atomic process. θ_i is the (N+1)th electron wave function with kinetic energy k_i^2 in a channel coupled with the core ion labeled as $S_iL_i(J_i)\pi_i k_i^2\ell_i[SL(J)\pi]$. A is the antisymmetrization operator. In the second term which is basically part of the first term, the Φ_js are bound channel functions of the (N+1)-electrons system that provides the orthogonality between the continuum and the bound electron orbitals and account for short range correlation. Substitution of $\Psi_E(e + ion)$ in the Schrodinger equation introduces a set of coupled equations that are solved by the R-matrix method. General descriptions of the R-matrix method can be found, e.g., in [11,12,42]. The energy eigenvalues from the R-matrix calculations are absolute and the (N+1)th electron can be bound or in the continuum depending on its negative or positive energy (E) The positive and negative energy states (Eq. (1)) define continuum or bound (e + ion) states,

$$\begin{aligned} E &= k^2 > 0 \longrightarrow \text{continuum (scattering) channel} \\ E &= -\frac{z^2}{\nu^2} < 0 \longrightarrow \text{bound state,} \end{aligned} \tag{7}$$

where ν is the effective quantum number relative to the core level. Determination of the quantum defect ($\mu(\ell)$), defined as $\nu_i = n - \mu(\ell)$ where ν_i is relative to the core level $S_iL_i\pi_i$, is helpful in establishing the ℓ-value associated with a given channel level.

The two methods treats the energy calculations differently. The energy eigenvalues in the R-matrix method are obtained from the poles of the Hamiltonian matrix formed by core ion and the outer interacting electron. The R-matrix method involves couplings of large number of channels and percentage contributions are determined from the outer region of the R-matrix boundary. These make it difficult to identify the spectroscopic designation for a state. However, it calculates the effective quantum number of each bound channel. Theoretical spectroscopy of the energy levels are carried out post BPRM calculations using an algorithm based on quantum defect theory incorporated in program PRECBPID [29,43,44]. It requires several considerations such as quantum defects, percentage of channel contributions, and angular momentum algebra, as explained in detail in Nahar [44]. Hund's rule is used as a guidance for levels arising from the same configuration such that a level with higher spin multiplicity ($2S + 1$) and higher orbital angular momentum L lies lower than that with lower spin multiplicity and lower total orbital angular momentum. Hence, the same level can have two different designations from atomic structure and from BPRM calculations considering channel percentage contributions in the methods. In principle both designations should be correct as both are possible designations, but with different percentage contributions.

The levels are designated as $C_t(S_tL_t\pi_t)J_t nl J \; SL\pi$, where C_t, $S_tL_t\pi_t$, J_t are the configuration, LS term, parity, and total angular momentum of the target or the core ion, and nl are the principal and orbital quantum numbers of the outer or the valence electron. J and $SL\pi$ are the total angular momentum, LS term and parity of the $(N+1)$-electron system.

Atomic structure computation using SS treat electrons as Fermi sea, constrained by Pauli exclusion principle, fill in cells up to a highest Fermi level. Based on quantum statistics, the TFDA model gives a continuous function $\phi(x)$ such that the potential is given by [37,42]

$$V(r) = -\frac{Z}{r}\phi(x), \phi(x) = e^{-Zr/2} + \lambda_{nl}(1 - e^{-Zr/2}), \; x = \frac{r}{\mu}, \tag{8}$$

$\mu = 0.8853\left(\frac{N}{N-1}\right)^{2/3}Z^{-1/3}$ = constant. Thomas–Fermi orbital scaling parameters λ_{nl} impacts on the expanding or compressing the orbital functions but maintains the right number of nodes and the orthogonality condition. An equivalent Schrodinger equation with $\phi(x)$ yields the solution in Whittaker functions computed numerically.

In contrast to BPRM, the number of possible states in an atomic structure calculation is predetermined from the set of configurations specified in the calculation. Spectroscopic identification of any state is selected by the highest leading percentage contribution as determined from the mixing coefficients of contributing states. Hence no theoretical spectroscopy is needed post the structure calculations.

There are a few differences between the two approaches, BPRM and SS. BPRM computes the absolute energies and the sign of the energy changes as it goes from bound to continuum. SS computes energy values relative to the ground state, and does not specify whether a state is crossing the ionization threshold in the continuum. The wavefunction in SS is similar to the first term of CC expansion, but all core ion orbital functions are directly multiplied by the outer electron orbital and the sum is over the configurations producing a specific state and thus includes contributions of multi-configurations interactions. While BPRM can generate a much larger set of transitions with $n \leq 10$, SS can compute transitions for n going to up to 5 or 6. The accuracy of SS is comparable to that of Dirac–Fock approximation for most ions. R-matrix can provide higher accuracy as it can accommodate a much larger set of configurations.

2.3. Transition probabilities

The probability for transition from state i to j, P_{ij}, due to a photon absorption is given by (e.g. [42])

$$P_{ij} = 2\pi \frac{c^2}{h^2 \nu_{ji}^2} | <j| \frac{e}{mc} \hat{\mathbf{e}} \cdot \mathbf{p} e^{i\mathbf{k}\cdot\mathbf{r}} |i> |^2 \rho(\nu_{ji}). \tag{9}$$

where k is the wave vector, ν_{ij} is the photon frequency for transition, ρ is the radiation density along with other standard constants. Various terms in $e^{i\mathbf{k}\cdot\mathbf{r}}$ introduce various multipole transitions, such as, the first term gives the electric dipole transitions E1, the second term gives E2 and M1, and the third term E3 and M2. The general line strength of a transition is obtained from

$$S^{X\lambda}(ij) = \left| \langle \Psi_j \| O^{X\lambda} \| \Psi_i \rangle \right|^2, \qquad S(ji) = S(ij). \tag{10}$$

where $O^{X\lambda}$ is the operator for various transitions Xλ. We report transitions of E1 in BPRM method and up to the third term in SS calculations. For E1 transitions, oscillator strengths, radiative decay rate which is also known as transition probability or Einstein's A-coefficient, and the corresponding photo-absorption cross sections can be obtained as

$$f_{ij} = \frac{E_{ji}}{3g_i} S^{E1}(ij), \quad A_{ji}^{E1} = \alpha^3 \frac{g_i}{g_j} E_{ji}^2 f_{ij}, \quad \sigma_{PI}(\nu) = 8.064 \frac{E_{ij}}{3g_i} S^{E1} \text{ [Mb]},$$

$$\tag{11}$$

where E_{ji} is the transition energy, ν is the photon energy, and α is the fine structure constant, g_j and g_i being the statistical weights of the upper and lower states respectively. The radiative decay rates for higher order multipole radiation electric quadrupole (E2) and magnetic dipole (M1) can be obtained as (e.g. [41])

$$g_j A_{ji}^{E2} = 2.6733 \times 10^3 \text{s}^{-1} (E_j - E_i)^5 S^{E2}(i,j) \tag{12}$$

$$g_j A_{ji}^{M1} = 3.5644 \times 10^4 \text{s}^{-1} (E_j - E_i)^3 S^{M1}(i,j); \tag{13}$$

and for electric octopole (E3) and magnetic quadrupole (M2) as

$$g_j A_{ji}^{E3} = 1.2050 \times 10^{-3} \text{s}^{-1} (E_j - E_i)^7 S^{E3}(i,j) \tag{14}$$

$$g_j A_{ji}^{M2} = 2.3727 \times 10^{-2} \text{s}^{-1} (E_j - E_i)^5 S^{M2}(i,j). \tag{15}$$

The lifetime of a level k can be computed as

$$\tau_k = \frac{1}{\sum_i A_{ki}} \tag{16}$$

In cgs units,

$$A_{ji}(s^{-1}) = \frac{A_{ji}(a.u.)}{\tau_0}, \tag{17}$$

where $\tau_0 = 2.4191 \times 10^{-17}$s is the atomic unit of time.

Observed energies are more precise than the calculated values and provide more accurate transition energies. To match with observations, which are determined by the measured energies, the transition parameters, particularly for E1 transitions, of both Fe V and Fe VI have been adjusted to the available observed energies. Using the energy independent BPRM line strength, S, and the observed energy E(obs), the f-value for dipole allowed transition can be obtained as,

$$f_{ij} = S(i, j, BPRM) \frac{E_{ji}(obs)}{(3g_i)}. \tag{18}$$

3. Computations

3.1. The BPRM calculations

As mentioned earlier, for the present results for Fe V and Fe VI are related. The R-matrix computations is initiated with the wavefunction expansion of the core ion. For the core ion, Fe VI, program SS [41] has been used to obtain the energies, transitions, and wavefunctions. These wavefunction for Fe VI are used to initiate the R-matrix calculations for Fe V. Hence atomic structure calculations for Fe VI is discussed first before the BPRM calculations for Fe V.

3.2. Atomic structure calculations for Fe VI

We use an optimized set of 9 configurations of Fe VI (listed in Table 1) for running the later version of the atomic structure code SS [41] for energies, allowed and forbidden transition, and wavefunctions. This configuration set is different from the set used earlier [30,43] for radiative data for Fe V, and includes orbital 4f not considered before. The optimized set of Thomas–Fermi scaling parameters (λ_{nl}) for the nl orbitals are also presented in Table 1. These were adjusted such that an overall agreement between a wider range of calculated and observed energies is achieved. Table 1 presents a set of calculated energies.

All atomic data for energies and transitions obtained from SS are processed through a code PRCSS, e.g. [45] to generate clear tables of energies and transitions of types E1, E2, E3, M1, and M2. The typical name of the output file of PRCSS containing these tables is EFBPSS.ion. The program is also used for processing transition rates where calculated energies are replaced by the available observed energies. It calculates the transition parameters using the calculated line strengths and the observed transition wavelengths.

Lifetimes of all excited levels were obtained using code LIFETMSS.f (e.g. Nahar [46]). Program sums up contributions of all A-values for allowed and forbidden transitions that decay to lower levels and take the inverse for the lifetime values of the excited levels.

The synthetic photo-absorption spectrum of the ion is generated by program SPECTRUM, e.g. Nahar [47], which takes the data from file EFBPSS.ion and calculates the photoabsorption cross sections of entire energy range and add those cross sections which have the same transition wavelengths.

3.3. BPRM calculations for Fe V

BPRM computations are carried out in a number of stages using a package of codes [17,18]. The first stage code, STG1, computes the one- and two-electron radial integrals using the one-electron target orbitals generated by SS.

Table 1 presents the 19 levels of Fe VI that were included in Fe V wavefunction. There is a large energy gap for excitation from 0.66 Ry of the 19th level of configuration $3d^3$ to about 2.4 Ry for the 20th level of configuration $3d^2 4s$. No bound state of Fe V is found to form with core excitation beyond the 19th level. This is the reason for choosing 19 level CC calculations for Fe V transitions.

Table 1

Energies of Fe VI obtained using SS [37,41] from an optimized set of 9 configurations, $3s^23p^63d^3$(1), $3s^23p^63d^24s$(2), $3s^23p^63d^24p$(3), $3s^23p^63d^24d$(4), $3s^23p^63d^24f$(5), $3s^23p^53d^4$(6), $3s3p^63d^4$(7), $3p^63d^5$(8), $3s^23p^43d^5$(9) with filled orbitals $1s^22s^22p^6$ in each configuration. The Thomas–Fermi orbital scaling parameters (λ_{nl}) used are 1.20(1s), 1.20(2s), 1.15(2p), 1.15(3s), 1.15(3p), 1.10(3d), 1.0(4s), 1.0(4p), 1.0(4d), 1.0(4f). The top 19 levels of Fe VI are used in the CC wavefunction of Fe V. The calculated energies (E_t) from SS are compared with those of Sugar and Corliss [24] available at NIST compilation table [25].

	Fe VI				
	Level		J_t	E_t(Ry) NIST	E_t(Ry) SS
1	3d3	^4F	1.5	0.0000E+00	0.0000E+00
2	3d3	^4F	4.5	1.8225E−02	2.2532E−02
3	3d3	^4F	3.5	1.0826E−02	1.3304E−02
4	3d3	^4F	2.5	4.6566E−03	5.6942E−03
5	3d3	^4P	2.5	1.7870E−01	1.9219E−01
6	3d3	^4P	1.5	1.7261E−01	1.8472E−01
7	3d3	^4P	0.5	1.7075E−01	1.8301E−01
8	3d3	^2G	4.5	1.9424E−01	3.0056E−01
9	3d3	^2G	3.5	1.8787E−01	2.0826E−01
10	3d3	^2P	1.5	2.3888E−01	2.7055E−01
11	3d3	^2P	0.5	2.4144E−01	2.5009E−01
12	3d3	^2D	2.5	2.5957E−01	2.6851E−01
13	3d3	^2D	1.5	2.6087E−01	2.4568E−01
14	3d3	^2H	5.5	2.6611E−01	3.0633E−01
15	3d3	^2H	4.5	2.6175E−01	2.1614E−01
16	3d3	^2F	3.5	4.2116E−01	4.6198E−01
17	3d3	^2F	2.5	4.2468E−01	4.6519E−01
18	3d3	^2D	2.5	6.5344E−01	6.8904E−01
19	3d3	^2D	1.5	6.5655E−01	6.9299E−01
			....		
20	$3d^2(^3F)4s$	^4F	4.5 23	2.471E+00	2.407E+00
21	$3d^2(^3F)4s$	^4F	3.5 22	2.462E+00	2.398E+00
22	$3d^2(^3F)4s$	^4F	2.5 21	2.454E+00	2.391E+00
23	$3d^2(^3F)4s$	^4F	1.5 20	2.449E+00	2.386E+00
24	$3d^2(^3F)4s$	^2F	3.5 25	2.529E+00	2.466E+00
25	$3d^2(^3F)4s$	^2F	2.5 24	2.514E+00	2.453E+00
26	$3d^2(^1D)4s$	^2D	2.5 26	2.648E+00	2.560E+00
27	$3d^2(^1D)4s$	^2D	1.5 27	2.650E+00	2.563E+00
28	$3d^2(^3P)4s$	^4P	2.5 30	2.671E+00	2.578E+00
29	$3d^2(^3P)4s$	^4P	1.5 29	2.663E+00	2.570E+00
30	$3d^2(^3P)4s$	^4P	0.5 28	2.659E+00	2.565E+00
31	$3d^2(^3P)4s$	^2P	1.5 32	2.725E+00	2.630E+00
32	$3d^2(^3P)4s$	^2P	0.5 31	2.717E+00	2.624E+00
33	$3d^2(^1G)4s$	^2G	4.5 33	2.745E+00	2.664E+00
34	$3d^2(^1G)4s$	^2G	3.5 34	2.745E+00	2.664E+00
35	$3d^2(^3F)4p$	$^4G^o$	5.5 43	3.159E+00	3.123E+00
36	$3d^2(^3F)4p$	$^4G^o$	4.5 40	3.148E+00	3.107E+00
37	$3d^2(^3F)4p$	$^4G^o$	3.5 38	3.138E+00	3.094E+00
38	$3d^2(^3F)4p$	$^4G^o$	2.5 35	3.130E+00	3.082E+00
39	$3d^2(^3F)4p$	$^4F^o$	4.5 42	3.159E+00	3.120E+00
40	$3d^2(^3F)4p$	$^4F^o$	3.5 41	3.149E+00	3.111E+00
41	$3d^2(^3F)4p$	$^4F^o$	2.5 39	3.142E+00	3.101E+00
42	$3d^2(^3F)4p$	$^4F^o$	1.5 37	3.136E+00	3.094E+00
43	$3d^2(^3F)4p$	$^2F^o$	3.5 48	3.176E+00	3.131E+00
44	$3d^2(^3F)4p$	$^2F^o$	2.5 44	3.164E+00	3.122E+00
45	$3d^2(^3F)4p$	$^4D^o$	3.5 50	3.186E+00	3.148E+00

Table 1 also compares the energies of the levels obtained using SS with the measured values of Sugar and Corliss [24]. The comparison shows larger discrepancies at lower energies. This is partly artificial since the energies are relative to zero energy of the ground state. With absolute values, which are larger numbers, of the energies the percent difference will be lower. The differences of small energies typically do not have much impact on transition parameters. The agreement between calculated and observed energies improves to less than a few percents for most higher levels. In the computations, the calculated energies were replaced by available observed energies so that energy positions of resonant series match the observed positions.

In the first term of the wavefunction expansion, Eq. (6), the N-electron states were multiplied by that of the interacting electron for which partial wave angular momenta ranged from 0 to 11. R-matrix basis set inside the R-matrix boundary for each orbital contained 12 terms. A larger R-matrix boundary with of radius $6.5a_o$ was chosen so that the amplitude of the R-matrix orbitals drops to almost zero at the boundary.

The second term of CC wavefunction expansion of Fe V contained 33 configurations of (N+1) electrons system with minimum and maximum occupancy as specified within parentheses of the orbitals, 1s(2-2), 2s(2-2), 2p(6-6), 3s(1-2), 3p(5-6), 3d (1-6), 4s(0-2), 4p(0-2), 4d(0-1), 4f (0-1).

STG2 computes the angular momenta algebra of dipole matrix elements in LS coupling. Conversion to intermediate coupling is carried out in a pair-coupling representation in stage RECUPD. The computer memory requirement for this stage has been the maximum as it carries out angular algebra of dipole matrix elements of a large number of levels due to fine-structure splitting. The (e + Fe VI) Hamiltonian is diagonalized for each resulting $J\pi$ in STGH. The Breit–Pauli calculations for Fe V considered all possible fine-structure bound levels with $(2S + 1) = 1, 3, 5$ and $L = 0 - 10$, $n \leq 10$, $\ell \leq n - 1$, and $J \leq 10$, and the transitions among these levels.

The bound energies were computed using code STGB. As mentioned in Theory section that the energies are scanned with small energy mesh in terms of effective quantum number mesh for poles in the Hamiltonian. The mesh was chosen very small, $\Delta\nu = 0.00025$, so that all poles are found. The computational requirements were, therefore increased considerably for the intermediate coupling over the LS coupling case by several orders of magnitude. The calculations take up to several CPU hours per $J\pi$ in order to determine the corresponding eigenvalues in the asymptotic program STGB. Transition parameters were processed by program PBPRAD, e.g. Nahar [44]. All energies were identified spectroscopically using the algorithm in program PRCBPID (e.g. [44]) mentioned in the Theory section. It took several months to carry out the spectroscopic identifications of 4300 fine structure levels. Line strengths, oscillator strengths, and radiative decay rate for bound–bound transitions were obtained using code STGBB.

Program LIFETMBP, e.g. [22], was used to compute the lifetimes of all excited levels. It lists all transitions, both allowed and forbidden, contributing to determine the lifetimes.

Program, SPECTRUM (e.g. [48]), was used to compute the spectral lines of the ions. The program added the photo-excitation cross sections that appear at the same transition energy for the final plot.

4. Results and discussions

We present extensive sets of radiative transitions corresponding to large sets of energies with spectral features of Fe V and Fe VI. All energies and transitions from BPRM calculations have been identified spectroscopically. Fe V, we present E1 transitions. Forbidden E2 and M1 transitions in Fe V are available at Nahar et al. [30]. All complete files of data for energies, oscillator strengths, lifetimes, and spectral points are available electronically at the database NORAD-Atomic-Data [21].

The energies, oscillator strength, lifetimes of both Fe V and Fe VI are discussed and compared with available values. While accuracy of data can be estimated from energies and single transition parameter, lifetimes of excited levels can also provide an estimated accuracy. Lifetimes are calculated by summing the A-values for all lower level transitions and taking its inverse.

Results of each ion is discussed separately below

4.1. Fe V results from BPRM method

4.1.1. Energies of Fe V

We present 4300 bound fine structure levels of Fe V obtained in relativistic Breit–Pauli R-matrix (BPRM) method. This number is over 400 higher than the earlier 3865 energy levels obtained using a different close coupling wavefunction expansion. Splitting of each LS term of the core ion into its fine-structure components increases the number of Rydberg series of levels converging on to the fine structure level.

Table 2

Sample table of Fe V energies in Ry where fine structure levels are ordered in energy values and are grouped together for their corresponding LS terms.

$C_t(S_tL_t\pi_t)$	J_t	nl	J	E(cal)	ν	$SL\pi$
Eqv electron/unidentified levels, parity: e						
3d4			0	−5.51320E+00	2.13	5D e
3d4			1	−5.51190E+00	2.13	5D e
3d4			2	−5.50940E+00	2.13	5D e
3d4			3	−5.50580E+00	2.13	5D e
3d4			4	−5.50150E+00	2.13	5D e
Nlv(c) = 5: set complete						
Nlv = 5, $^5L^e$:F (5 4 3 2 1)						
3d3	(4Fe)	3/2 4s	1	−3.81430E+00	2.57	5F e
3d3	(4Fe)	5/2 4s	2	−3.81160E+00	2.57	5F e
3d3	(4Fe)	5/2 4s	3	−3.80770E+00	2.57	5F e
3d3	(4Fe)	7/2 4s	4	−3.80250E+00	2.57	5F e
3d3	(4Fe)	9/2 4s	5	−3.79640E+00	2.57	5F e
Nlv(c) = 5: set complete						

Table 3

Sample table of Fe V energies in Ry listed in $J\pi$ symmetry order for easy incorporation to models. The energies are also ordered.

i	Conft	SLpt	Jt	nl	J	E(Ry)	EQN	Terms
Nlv = 84, J pi = 0 e								
1	3d4				0	−5.51320E+00	2.13	^5De
2	3d4				0	−5.29400E+00	2.17	^3Pe
3	3d4				0	−5.05670E+00	2.22	^1Se
4	3d4				0	−4.93520E+00	2.25	^3Pe
5	3d4				0	−4.40930E+00	2.38	^1Se
6	3d3	$^4P^e$	1/2	4s	0	−3.57630E+00	2.60	^3Pe
7	3d3	$^2P^e$	1/2	4s	0	−3.49040E+00	2.59	^3Pe
8	3d3	$^4F^e$	3/2	4d	0	−2.18889E+00	3.38	^5De
9	3d3	$^4F^e$	5/2	4d	0	−2.14737E+00	3.41	^3Pe
10	3d3	$^4P^e$	3/2	4d	0	−1.99336E+00	3.40	^5De
11	3d3	$^4P^e$	5/2	4d	0	−1.97023E+00	3.41	^3Pe
12	3d32	$^2D^e$	3/2	4d	0	−1.91601E+00	3.46	^3Pe
13	3d3	$^2P^e$	3/2	4d	0	−1.84965E+00	3.46	^3Pe
14	3d3	$^2F^e$	5/2	4d	0	−1.75517E+00	3.52	^3Pe

These result in a large number of fine-structure levels in comparatively narrow energy bands.

All energies have been spectroscopically identified uniquely using an algorithm [29,43,44] mentioned in the Theory section. An energy level in a set of fine structure levels corresponding to more than a LS term, can have more than one possible designation. As suggested, Hund's rule can be followed for further for distribution of designations. Identification of levels and group them to belonging to LS terms can be varied within correct physics. Tables 2 and 3 provide samples of complete energy tables, available online, presented in two useful formats, (i) fine structure levels as sets of components of LS terms for various comparisons and (ii) in $j\pi$ symmetry for incorporation to models. Note that the value of effective quantum number (EQN = ν) should be avoided since nl may have changed during spectroscopy processing.

Fe V energies are compared with 179 measured values [24,25]. Except one, all energies agree within less than 1 to less than 5% with the observed energies. Part of comparison is presented in Table 4.

We have used very fine mesh of effective quantum number ($\Delta\nu = 0.00028$) to scan for all bound levels. Even with it, some high lying levels were missed. Further fine tuning of $\Delta\nu$ was not possible as it brought numerical instability.

4.1.2. E1 transitions in Fe V from BPRM method

We have obtained an extensive set of 1.71×10^6 E1 transitions among the 4300 bound fine structure levels of Fe V. This number is significantly higher than the previous set of 1.46×10^6 transitions [30]. The format of presenting the present data is similar to the previous one. Table 5 presents a sample set of transitions to demonstrate the format adopted for the complete set of oscillator strengths, energies.

Table 4

Comparison of the present calculated fine structure energies of Fe V with those of Sugar and Corliss [24] available in the compilation table of the NIST [25]. Number next to a J value specifies its position in the energy set of the $J\pi$ symmetry.

Fe V: $N_{BPRM} = 4300$

Configuration	Level	J	E_{NIST}(Ry)	E_{BPRM}(Ry)
3d4	^5D	4.0 1	5.502E+00	5.449E+00
3d4	^5D	3.0 1	5.506E+00	5.454E+00
3d4	^5D	2.0 1	5.509E+00	5.457E+00
3d4	^5D	1.0 1	5.512E+00	5.460E+00
3d4	^5D	0.0 1	5.513E+00	5.462E+00
3d42	^3P	2.0 2	5.272E+00	5.197E+00
3d42	^3P	1.0 2	5.286E+00	5.205E+00
3d42	^3P	0.0 2	5.294E+00	5.214E+00
3d4	^3H	6.0 1	5.280E+00	5.219E+00
3d4	^3H	5.0 1	5.283E+00	5.223E+00
3d4	^3H	4.0 2	5.286E+00	5.226E+00
3d42	^3F	4.0 3	5.267E+00	5.194E+00
3d42	^3F	3.0 2	5.269E+00	5.196E+00
3d42	^3F	2.0 3	5.269E+00	5.191E+00
3d4	^3G	5.0 2	5.236E+00	5.168E+00
3d4	^3G	4.0 4	5.238E+00	5.170E+00
3d4	^3G	3.0 3	5.242E+00	5.174E+00
3d42	^1G	4.0 5	5.180E+00	5.099E+00
3d4	^3D	3.0 4	5.179E+00	5.102E+00
3d4	^3D	2.0 4	5.178E+00	5.101E+00
3d4	^3D	1.0 3	5.177E+00	5.099E+00
3d4	^1I	6.0 2	5.171E+00	5.106E+00
		...		

Table 5

Sample set of transition probabilities demonstrating the format of the data in the file containing the complete set of transitions. The energy levels with $J\pi$ and index 'iii' is listed above the table of transitions so they can match those of the transitional levels.

```
Energy table:

 i   j  p iiii     E(Ry)      conf        LS term    jjpiiii

 1  0.0 e   1   -5.51320E+00  3d4           5De            1
 2  0.0 e   2   -5.29400E+00  3d4       2   3Pe            2
 3  0.0 e   3   -5.15200E+00  3d4       2   1Se            3
 4  0.0 e   4   -4.93520E+00  3d4       1   3Pe            4
 5  0.0 e   5   -4.40930E+00  3d4       1   1Se            5
     ........

Table of fL=Oscillator strengths, S=line strengths, A=A-value

  26   22 : Z, Number of electrons

 i   j    wl(A)   Ei(Ry)     Ej(Ry)      fL        S       Aji(s-1)

 1   0    3   1     84  256  21504 : gi Pi gf Pf Ni Nf NN
 1   1  387.97 -5.5132E+00 -3.1644E+00 -1.726E-01  2.243E-01  2.462E+09
 1   2  386.26 -5.5132E+00 -3.1540E+00 -2.448E-02  3.175E-02  3.508E+08
 1   3  384.61 -5.5132E+00 -3.1439E+00 -7.178E-02  9.266E-02  1.038E+09
 1   4  365.43 -5.5132E+00 -3.0195E+00 -8.493E-02  1.031E-01  1.390E+09
 1   5  363.43 -5.5132E+00 -3.0058E+00 -4.874E-03  5.877E-03  8.079E+07
 1   6  361.31 -5.5132E+00 -2.9911E+00 -2.208E-03  2.650E-03  3.693E+07
 1   7  354.68 -5.5132E+00 -2.9439E+00 -5.401E-04  6.328E-04  9.481E+06
 1   8  352.41 -5.5132E+00 -2.9274E+00 -1.938E-06  2.260E-06  3.433E+04
 1   9  349.69 -5.5132E+00 -2.9073E+00 -8.259E-05  9.554E-05  1.487E+06
 1  10  349.41 -5.5132E+00 -2.9052E+00 -3.153E-05  3.645E-05  5.685E+05
-----------------------------------------------------------------
```

The complete set of energies is listed with configuration, terms, and indices that correspond those in the table of transitions is provided at the beginning of the file. This enables spectroscopic identification of transitions. Below the energy table are the sets of transitions belonging to a pair of symmetries $J\pi - J'\pi'$. The two numbers at the beginning of the transition table are the nuclear charge (i.e. Z = 26) and the number of electrons ($N_{elc} = 22$) in the ion. The first line of each set contains values of $2J+1$, parity π (=0 for even and =1 for odd) of the transitional levels. Hence in Table 5, the first line gives the set of transitions given are among $J = 0^e - J = 1°$ levels, number of bound levels, N_i and N_f, in each symmetry and the total number $NN = N_i \times N_f$ of transitions in the set. This line is followed by NN transitions. The first two columns are the level indices, I_i and I_j (iii numbers of the symmetries) for the

Table 6

Comparison of present f-values with the earlier ones. The numbers I_i and I_j indicate positions of the levels in the series of levels of $SL\pi$.

C_i	C_j	$S_iL_i\pi_i$	$S_jL_j\pi_j$	$2J_i+1$	I_i	$2J_j+1$	I_j	$f_{ij}(P)$	$f_{ij}(others)$
$3d^4$	$-3d^3(^4F)4p$	^5D	$^5F^o$	1	1	3	1	0.1726	0.163[a], 0.1366[b]
$3d^4$	$-3d^3(^4F)4p$	^5D	$^5F^o$	5	1	3	1	0.1270	0.0126[a]
$3d^4$	$-3d^3(^4F)4p$	^5D	$^5F^o$	5	1	5	3	0.05432	0.0596[a]
$3d^4$	$-3d^3(^4F)4p$	^5D	$^5F^o$	5	1	7	3	0.02556	0.0138[a]
$3d^4$	$-3d^3(^4F)4p$	^5D	$^5F^o$	7	1	5	3	0.02177	0.0274[a]
$3d^4$	$-3d^3(^4F)4p$	^5D	$^5F^o$	7	1	7	3	0.04339	0.0544[a]
$3d^4$	$-3d^3(^4F)4p$	^5D	$^5F^o$	9	1	7	3	0.004821	0.00756[a]
$3d^4$	$-3d^3(^4F)4p$	^5D	$^5F^o$	7	1	9	3	0.05659	0.0414[a]
$3d^4$	$-3d^3(^4F)4p$	^5D	$^5F^o$	9	1	9	3	0.01757	0.03[a]
$3d^4$	$-3d^3(^4F)4p$	^5D	$^5F^o$	9	1	11	2	0.07290	0.0686[a]
$3d^4$	$-3d^3(4F)4p$	^5D	$^5D^o$	1	1	3	2	0.0245	0.041[a], 0.0702[b]
$3d^4$	$-3d^3(^4F)4p$	^5D	$^5D^o$	3	1	1	1	0.06047	0.0607[a], 0.041[b]
$3d^4$	$-3d^3(^4F)4p$	^5D	$^5D^o$	3	1	3	2	0.0345	0.0343[a]
$3d^4$	$-3d^3(^4F)4p$	^5D	$^5D^o$	3	1	5	2	0.1207	0.1257[a]
$3d^4$	$-3d^3(^4F)4p$	^5D	$^5D^o$	5	1	3	2	0.04630	0.0532[a]
$3d^4$	$-3d^3(^4F)4p$	^5D	$^5D^o$	5	1	5	2	0.01522	0.0092[a]
$3d^4$	$-3d^3(^4F)4p$	^5D	$^5D^o$	5	1	7	2	0.08956	0.1006[a]
$3d^4$	$-3d^3(^4F)4p$	^5D	$^5D^o$	7	1	5	2	0.03037	0.0247[a]
$3d^4$	$-3d^3(^4F)4p$	^5D	$^5D^o$	7	1	7	2	0.06331	0.0517[a]
$3d^4$	$-3d^3(^4F)4p$	^5D	$^5D^o$	9	1	7	2	0.02478	0.0222[a]
$3d^4$	$-3d^3(^4F)4p$	^5D	$^5D^o$	7	1	9	2	0.04739	0.0588[a]
$3d^4$	$-3d^3(^4F)4p$	^5D	$^5D^o$	9	1	9	2	0.1427	0.130[a]
$3d^4$	$-3d^3(^4P)4p$	^5D	$^5P^o$	1	1	3	4	0.08493	0.076[a], 0.0755[b]
$3d^4$	$-3d^3(^4P)4p$	^5D	$^5P^o$	3	1	3	4	0.06390	0.057[a]
$3d^4$	$-3d^3(^4P)4p$	^5D	$^5P^o$	3	1	5	6	0.02089	0.019[a]
$3d^4$	$-3d^3(^4P)4p$	^5D	$^5P^o$	5	1	3	4	0.02994	0.0266[a]
$3d^4$	$-3d^3(^4P)4p$	^5D	$^5P^o$	5	1	5	6	0.04920	0.0442[a]
$3d^4$	$-3d^3(^4P)4p$	^5D	$^5P^o$	5	1	7	7	0.00567	0.0054[a]
$3d^4$	$-3d^3(^4P)4p$	^5D	$^5P^o$	7	1	5	6	0.06695	0.0499[a]
$3d^4$	$-3d^3(^4P)4p$	^5D	$^5P^o$	7	1	7	7	0.02859	0.0264[a]
$3d^4$	$-3d^3(^4P)4p$	^5D	$^5P^o$	9	1	7	7	0.08570	0.0758[a]

[a] Fawcett [32].
[b] Aggarwal et al [33].

energy indices of the levels, the third column is the transition energy in Å, the fourth and fifth columns are their energies, E_i and E_j, in Rydberg units. The sixth column is oscillator strengths f_L, seventh is line strength S, and the eighth column is the radiative decay rate or transition probability A-value. For the f-values that are negative the lower level is i (absorption) and for the positive ones the lower level is j (emission).

We make comparison of the present oscillator strengths with earlier values of Fawcett [32] and Aggarwal et al. [33] in Table 6. The comparison shows various degrees of agreement. While transitions, such as, $3d^4(^5D_0) - 3d^3(^4F)4p(^5F_1^o)$, $3d^4(^5D_2) - 3d^3(^4F)4p(^5F_2^o)$, $3d^4(^5D_1) - 3d^3(^4F)4p(^5D_2^o)$, show good agreement among theories, $3d^4(^5D_4) - 3d^3(^4F)4p(^5F_4^o)$ and $3d^4(^5D_3) - 3d^3(^4F)4p(^5D_4^o)$, have larger differences (see Table 6). This is not entirely unexpected. Except for the lowest transitions, f-values from different approximations typically show inconsistency in agreement, sometime good and other times larger differences. The origin of such differences is the wavefunction representation of the methodologies and also proper identification of levels of multi-electron systems.

The present work reports obtaining lifetimes of all excited levels, 4299 in total, of Fe V. The file containing lifetime of each level along with list of the contributing decays to lower levels is available electronically at the database NORAD-Atomic-Data [21].

Some of the lifetimes of Fe V are reported in Table 7 where they are compared with available values. Dumont et al. [26] measured lifetimes of a number of levels of Fe V using beam-foil technique. They also report calculated lifetime obtained using calculated transition probabilities of Abbott [27] in collaboration with Biement and Ekberg [49]. Instead of including all possible transitions to lower levels, they include a single transition classified by Ekberg [49] to obtain the predicted lifetimes. Even with theoretical differences, both their and present predicted sets of lifetimes for $3d^3(^4F)4p^5F^o$ levels and $3d^3(^4F)4p^5D^o$ levels agree well with each other and are lower than the measured values. Even for levels of $3d^3(^2H)4p^3I^o$ they agree more with each

other except for the $3d^3(^2H)4p^3I_7^o$ level where present lifetime is closer to the measured value. For $3d^3(^4F)4p^5G^o$ levels, present lifetimes are closer to measured values than the calculated values they present. The predicted lifetime of their identified level $(a^2D)^3F_4^o$ agrees well with the present lifetime of the level of same symmetry but with core state ^4F. This could be a misidentification of level. With large of electrons, exact identification is an issue unless it has a clear dominant leading percentage. We can also assume that with higher number of possible decays, the sum of radiative decay rates, A-values, increases lowering the lifetimes of the level. Lifetimes of a level includes sum of all A-values from the level to lower levels. Hence summing decay rates to a larger number of lower levels can increase the sum of A-values significantly causing reduced lifetime of the level.

The f-values of 1.71×10^6 transitions in Fe V have been used to produce the synthetic photoabsorption spectrum of Fe V. The absorption features over the wavelength range from soft xray to infrared are detailed in Fig. 1. Panel (a) show the total spectrum of strength, panel (b) total dominant rage of visible line, and panel (c) shows the prominent region of sharp lines. The range indicates high observational detectability of lines from stars and astronomical objects by several observatories from X-ray to far-infrared wavelengths including James Webb Space telescope (JWST). This spectrum presents lines of bound–bound transitions, not any bound-free transition.

4.2. Fe VI results from SUPERSTRUCTURE

The results for energies and transitions Fe VI obtained from atomic structure calculations using the latest version of the program SUPERSTRUCTURE (SS) [41] are discussed separately in the sections below. As mentioned earlier the wavefunctions and energies of Fe VI, as presented here, have been used to represent the core ion wavefunctions and energies of Fe V for the BPRM calculations of the ion.
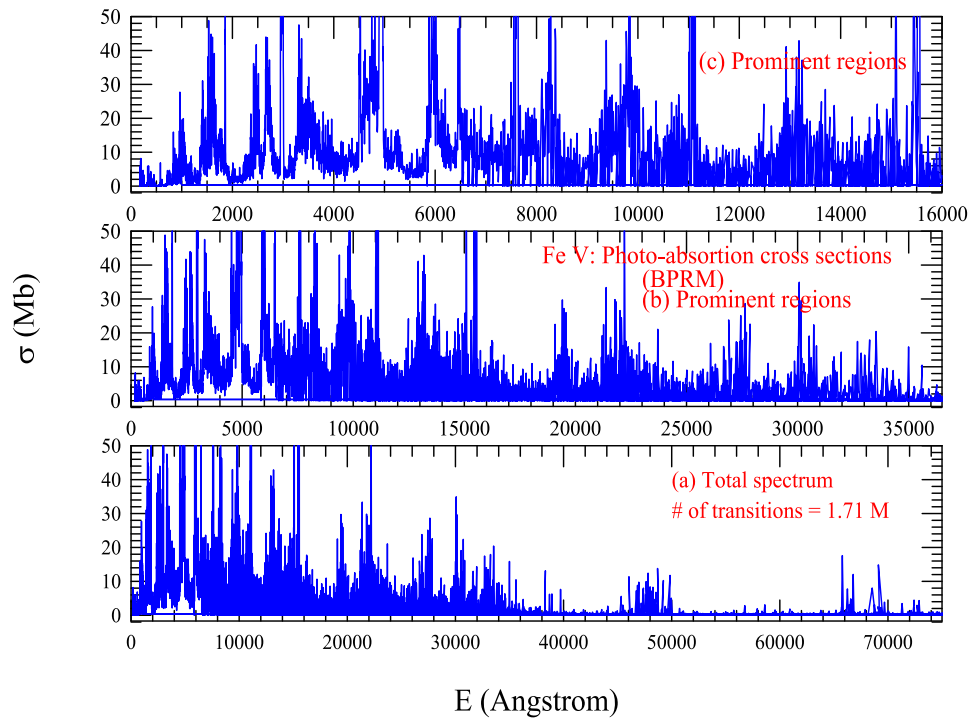
Fig. 1. Spectral features of Fe V: (a) total spectrum using present 1.71 million lines from bound-bound transitions, (b) Region of prominent lines, (c) region of strongest lines.

Table 7
Comparison of present lifetimes (τ) of Fe V with the earlier measured and calculated values.

Excited level	τ (nsec)		τ (nsec)
Transition[c]	Expt[a]	Theory[a,b]	Present
$(^4F)^5F_4 - (^4F)^5F_4^o$	0.52 ± 0.04		0.275
$(^4F)^5F_3 - (^4F)^5F_3^o$	0.52 ± 0.04		0.252
$(^4F)^5F_5 - (^4F)^5F_5^o$	0.54 ± 0.02	0.28	0.277
$(^4F)^5F_2 - (^4F)^5F_2^o$	0.54 ± 0.02	0.17	0.202
$(^4P)^5P_3 - (^4P)^5D_4^o$	1.2 ± 0.2	0.66	0.623
$(^2H)^3H_6 - (^2H)^3I_7^o$	0.9 ± 0.2	0.57	1.577
$(^2H)^3H_5 - (^2H)^3I_6^o$	0.9 ± 0.1	0.57	0.644
$(^2H)^3H_4 - (^2H)^3I_5^o$	0.9 ± 0.1	0.55	0.632
$(^2F)^5F_3 - (^4F)^5D_2^o$	0.3 ± 0.02	0.15	0.141
$(^2F)^5F_4 - (^4F)^5D_3^o$	0.3 ± 0.02	0.15	0.125
$(^2F)^5F_5 - (^4F)^5D_4^o$	0.3 ± 0.02	0.15	0.116
$(^4F)^5F_5 - (^4F)^5G_6^o$	1.4 ± 0.2	0.96	1.216
$(^4F)^5F_4 - (^4F)^5G_5^o$	1.5 ± 0.3	0.97	1.235
$(^4F)^5F_3 - (^4F)^5G_4^o$	1.5 ± 0.1	0.99	1.251
$(^4F)^5F_2 - (^4F)^5G_3^o$	1.7 ± 0.2		1.262
$(a^2D)^3D_3 - (a^2D)^3F_4^o$	0.4 ± 0.03	0.17	0.175

[a] Dumont et al [26].
[b] Abbot [27].
[c] c-Ekberg [49].

4.2.1. Energies of Fe VI

The present atomic structure calculations for Fe VI resulted in 1071 energy levels, including both bound and continuum, from the nine configurations, as listed in Table 1. All configurations produce bound levels except configuration, $3p^6 3d^5$, which did not produce any bound level. The present energies from SUPERSTRUCTURE (SS) [41] are available in tabular form at NORAD-Atomic-Data [21]. These energies are compared with the measured values of Sugar and Corliss [24,25] in Table 1 and are discussed in the Computation section.

4.3. E1, E2, E3, M1, M2 transitions in Fe VI

From 1071 levels, we have obtained a total of 506,512 transitions of Fe VI of which 101,893 transitions are of type allowed E1 and

404,619 are of forbidden types E2, E3, M1, M2. Allowed transitions are typically orders of magnitude higher than those of forbidden types. Transition parameters $S-$, $f-$, and $A-$ values for the allowed and forbidden transitions have been processed with transition energies in wavelengths and Rydberg levels in tabular forms and are available at NORAD-Atomic-Data [21].

Available transitions in Fe VI are much limited and are presented mainly for forbidden transitions. These transitions are related to electron impact excitation. Garstang et al. [38] and Nussbaumer and Storey [39] report E2 and M1 transitions. Chen and Pradhan [36] report both allowed E1 and forbidden E2,M1 transitions for 83 fine structure levels of Fe VI that they studied. Present transitions are compared with others in Table 8. We find that E1 transition with no spin change agree very well with those of Chen and Pradhan [36] but differences can be noted for the intercombination or E1 transitions where spin changes. Both works used SS, but different versions of it and with different set of configurations. Present work corresponds to the latest version of the code [41].

Forbidden transitions, E2 and M1, of the present work are also compared with the three available sources, [36,38,39] in Table 8. It can be seen that transition probabilities from all four calculations for both E2 and M1 transitions have very good agreement with each other for most cases. Some differences are seen with those of Garstang et al. [38].

We have calculated lifetimes of all excited levels of Fe VI. Similar to Fe V, the table of lifetimes of Fe VI contains contributions of all decay rates to each excited level. Table 9 compares present lifetimes with those available in literature. Present lifetime for $^2H_{9/2}^o$ level agree very well with the measured value. The rest of 4 values agree more with their predicted values. However, the present lifetime of level $2F_{5/2}^o$, 0.11 nanosec, is much lower than the experimental and other predicted values. The reason is difficult to explain except that present lifetime includes contributions of decays to 60 levels, of which 24 are allowed E1 and 36 are forbidden transitions. This could have increased the total A-value.

Table 8

Comparison of present f- and A-values with available ones.

Transition		A (s⁻¹)(E1) Present	Others
$3d^3 - 3d^2(^3F)4p$	$^4F_{3/2} - {}^4G^o_{5/2}$	1.03e+9	1.19e+09[a]
$3d^3 - 3d^2(^3F)4p$	$^4F_{3/2} - {}^4F^o_{3/2}$	8.23e+09	8.92e+09[a]
$3d^3 - 3d^2(^3F)4p$	$^4F_{3/2} - {}^4F^o_{5/2}$	1.21e+09	1.26e+09[a]
$3d^3 - 3d^2(^3F)4p$	$^4F_{3/2} - {}^4D^o_{1/2}$	9.05E+09	1.01e+10[a]
$3d^3 - 3d^2(^3P)4p$	$^4F_{3/2} - {}^4D^o_{1/2}$	3.7e+09	2.90e+09[a]
$3d^3 - 3d^2(^3F)4p$	$^4F_{5/2} - {}^4D^o_{3/2}$	6.18e+09	5.96e+09[a]
$3d^3 - 3d^2(^3F)4p$	$^4F_{3/2} - {}^2F^o_{5/2}$	1.06E+08	3.17e+07[a]
$3d^3 - 3d^2(^3P)4p$	$^4F_{3/2} - {}^2D^o_{3/2}$	8.47e+07	3.74e+06[a]
$3d^3 - 3d^2(^1G)4p$	$^4F_{7/2} - {}^2G^o_{9/2}$	8.71e+04	1.28e+04[a]

Transition Conf	Levels	A (s⁻¹)(E2) Present	Others	A (s⁻¹)(M1) Present	Others
$3d^3 - 3d^3$	$^4F_{5/2} - {}^4F_{3/2}$	4.58e−11	5.13e−11[a], 0.[b], 4.97−11[c]	5.75E−03	5.76e−3[a], 5.7e−3[b], 5.74e−3[c]
$3d^3 - 3d^3$	$^4P_{1/2} - {}^4F_{3/2}$	5.41e−02	6.04e−2[a], 8.3e−2[b], 5.97−2[c]	2.85E−04	2.01e−4[a], 8.0e−5[b], 3.31−4[c]
$3d^3 - 3d^3$	$^4P_{3/2} - {}^4F_{3/2}2$	1.14E−02	1.27e−2[a], 1.7e−2[b], 1.26e−2[c]	5.00E−03	3.40e−3[a], 1.2e−3i[b], 4.05e−3[c]
$3d^3 - 3d^3$	$^4P_{5/2} - {}^4F_{3/2}2$	6.41E−04	7.15e−4[a], 1.0e−3[b], 7.04e−4[c]	2.81E−04	2.15e−4[a], 9.0e−5[b], 2.66e−4[c]
$3d^3 - 3d^3$	$^2G_{7/2} - {}^4F_{3/2}2$	2.25E−05	1.90e−5[a], 1.4e−5[b], 0.0[c]	0.0	0.0[a], 1.4e−5[b], 1.66−5[c]
$3d^3 - 3d^3$	$^2P_{1/2} - {}^4F_{3/2}2$	2.20e−03	1.99e−3[a], 3 7.0e−3[b], 1.54e−3[c]	2.00E−03	1.54e−3[a], 7.3e−4[b], 1.99e−3[c]
$3d^3 - 3d^3$	$^2P_{3/2} - {}^4F_{3/2}2$	3.02E−04	6.88e−4[a], 2.8e−3[b], 5.40e−4[c]	3.19E−01	3.70e−1[a], 1.19e−1[b], 3.56e−1[c]
$3d^3 - 3d^3$	$^4F_{7/2} - {}^4F_{5/2}$	1.82e−10	2.03e−10[a], 0.[b], 1.99e−10[c]	1.34E−02	1.34e−2[a], 1.3e−2[b], 1.34e−2[c]
$3d^3 - 3d^3$	$^4F_{9/2} - {}^4F_{5/2}2$	5.87e−10	6.46e−10[a]	0	0.0[a]
$3d^3 - 3d^3$	$^4P_{1/2} - {}^4F_{5/2}2$	3.22e−02	3.47e−2[a], 4.85e−2[b], 0.[c]	0.0	0.0[a], 0.[b], 3.42e−2[c]
$3d^3 - 3d^3$	$^4P_{3/2} - {}^4F_{5/2}2$	2.99−02	3.35e−2[a], 4.59e−2[b], 3.32e−2[c]	3.03E−03	1.97e−3[a], 6e−4[b], 1.78e−3[c]
$3d^3 - 3d^3$	$^4P_{5/2} - {}^4F_{5/2}2$	5.11e−03	5.69e−3[a], 7.9e−3[b], 5.63e−3[c]	1.33E−03	9.87e−4[a], 4.2e−4[b], 1.36e−3[c]

[a] Chen and Pradhan [35].
[b] Garstang et al [38].
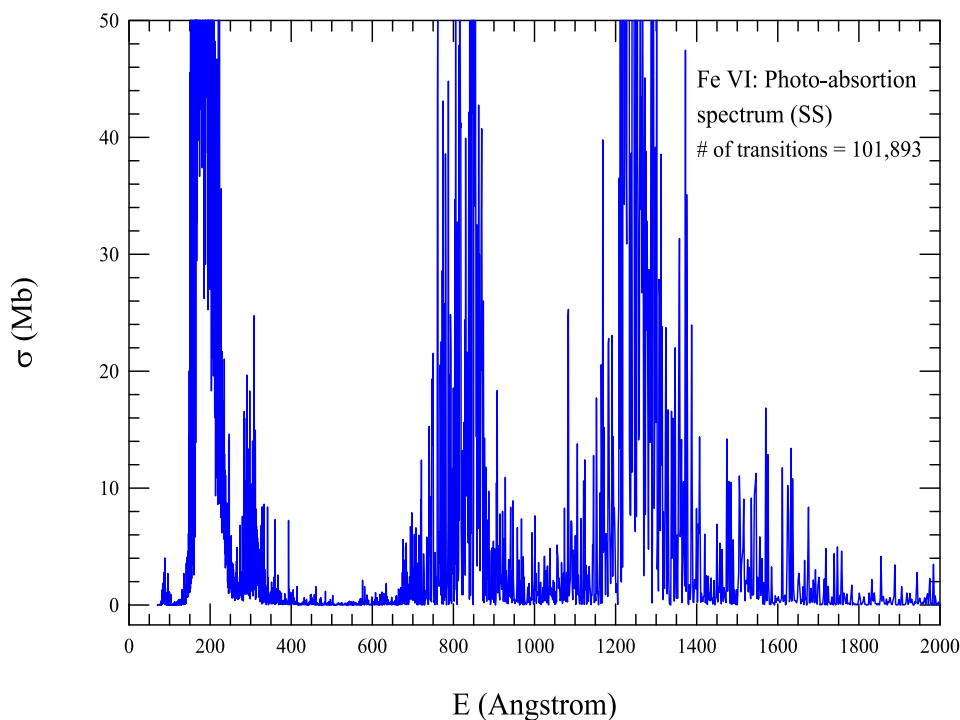[c] Nussbaumer and Storey [39].

Fig. 2. Spectral features of Fe VI demonstrating prominent region of strong lines in the x-ray and ultraviolet.

Fig. 2 presents the photoabsorption spectrum of Fe VI. This includes 101,893 lines of both bound–bound and bound-free transitions. The spectrum shows three regions of very strong lines, in the soft Xray about 100–300 Å, extreme ultraviolet of about 700–900 Å, and 1200–1400 Å. This spectrum presenting strong high energy lines in x-ray to ultraviolet region is much different from that of Fe V with a wider range of lines for detection.

5. Conclusion

Extensive sets of Level energies, fine-structure transition probabilities, lifetimes, and spectral features of Fe V and Fe VI are presented in a comprehensive manner.

Lifetimes of all excited levels of both Fe V and FE VI have been obtained.

Table 9

Comparison of present lifetimes (τ) of Fe VI with the earlier measured and calculated values.

Excitation Transition[c]	τ (nsec) Expt[a]	τ (nsec) Theory[a],[b]	Present
$(^1G)^2G_{7/2} - (^1G)^2H^o_{9/2}$	0.33 ± 0.03	0.18	0.315
$(^1G)^2G_{9/2} - (^1G)^2H^o_{11/2}$	0.33 ± 0.05	0.18	0.15
$(^3F)^4F_{9/2} - (^3F)^4G^o_{11/2}$	0.81 ± 0.06	0.45	0.39
$(^3F)^4F_{7/2} - (^3F)^4G^o_{9/2}$	0.62 ± 0.05	0.39	0.39
$(^3F)^4F_{5/2} - (^3F)^4G^o_{7/2}$	0.59 ± 0.05	0.41	0.39
$(^3F)^2F_{5/2} - (^3F)^2F^o_{5/2}$	0.59 ± 0.05	0.41	0.11

[a] Dumont et al [26].

[b] Abbot [27].

[c] Ekberg [50].

Theoretical spectroscopy was carried out for 4300 fine structure levels of Fe V for unique identifications.

These data to be particularly useful for the calculation of monochromatic opacities and in the analysis of spectra from astrophysical and laboratory sources.

Spectral features of both ions are illustrated. Fe V spectrum shows dominance of strong spectral lines over a wider range of wavelengths, from soft X-ray to infrared. In contrast, spectral features of Fe VI is confined to from X-ray to ultraviolet.

All data tables will be electronically available from the CDS archives, and from author's database NORAD-Atomic-Data at the Ohio State University.

Declaration of competing interest

Acknowledgments

Data availability

Data will be made available at NORAD-Atomic-Data (https://norad.astronomy.osu.edu/)

References

[1] D.E. Osterbrock, Astrophysics of Gaseous Nebulae and Active Galactic Nuclei, University Science Books, Mill Valley, 1989.

[2] M. Peimbert, in: S. Torres-Peimbert (Ed.), IAU Symp. 131, Planetary Nebulae, Reidel, Dordrecht, 1989, p. 577.

[3] M.A. Barstow, I. Hubeny, T. Lanz, J.B. Holberg, E.M. Sion, in: S. Bowyer, R.F. Malina (Eds.), Astrophysics in the Extreeme Ultraviolet, Kluwer, Dordrecht, 1996, p. 203.

[4] D. Koester, in: S. Bowyer, R.F. Malina (Eds.), Astrophysics in the Extreme Ultraviolet, Kluwer, Dordrecht, 1996, p. 185.

[5] S. Vennes, in: S. Bowyer, R.F. Malina (Eds.), Astrophysics in the Extreme Ultraviolet, Kluwer, Dordrecht, 1996, p. 193.

[6] M.J. Seaton, Yu Yan, D. Mihalas, A.K. Pradhan, Mon. Not. R. Astron. Soc. 266 (1994) 805.

[7] A.K. Pradhan, S.N. Nahar, W. Eissner, J. PHys. B: At. Mol. Opt. Phys. 57 (2024) 125001.

[8] M.J. Seaton, Mon. Not. R. Astron. Soc. 289 (1997) 700.

[9] M.J. Seaton, Mon. Not. R. Astron. Soc. 307 (1999) 1008.

[10] A. Hui-Bon-Hoa, G. Alecian, Astron. Astrophys. 332 (1998) 224.

[11] The Opacity Project Vol. 1, Institute of Physics Publishing, Bristol & Philadelphia, 1995.

[12] D.G. Hummer, K.A. Berrington, W. Eissner, A.K. Pradhan, H.E. Saraph, J.A. Tully, Astron. Astrophys. 279 (1993) 298.

[13] P.G. Burke, A. Hibbert, W.D. Robb, J. Phys. B 4 (1971) 153.

[14] N.S. Scott, P.G. Burke, J. Phys. B 12 (1980) 4299.

[15] N.S. Scott, K.T. Taylor, Comput. Phys. Comm. 25 (1982) 347.

[16] M.J. Seaton, J. Phys. B 20 (1987) 6363.

[17] K.A. Berrington, P.G. Burke, K. Butler, M.J. Seaton, P.J. Storey, K.T. Taylor, Yu Yan, J. Phys. B 20 (1987) 6379.

[18] K.A. Berrington, W.B. Eissner, P.H. Norrington, Comput. Phys. Comm. 92 (1995) 290.

[19] TOPbase, W. Cunto, C. Mendoza, F. Ochsenbein, C.J. Zeippen, Astron. Astrophys. 275 (1993) L5, url: https://cds.unistra.fr/topbase/topbase.html.

[20] TIPbase, url: https://cds.unistra.fr/tipbase/home.html.

[21] S.N. Nahar, Atoms 8 (4) (2020) 68; S.N. Nahar, G. Hinojosa-Aguirre, Atoms 12 (2024) 22, url: https://norad.astronomy.osu.edu/.

[22] S.N. Nahar, Astron. Astrophys. 293 (1995) 967.

[23] S.N. Nahar, A.K. Pradhan, Astron. Astrophys. Suppl. Ser. 135 (1999) 347.

[24] J. Sugar, C. Corliss, J. Phys. Chem. Ref. Data 14 (Suppl. 2) (1985).

[25] NIST, A. Kramida, Yu Ralchenko, J. Reader, NIST ASD Team, Atomic Spectra Database (Ver. 5.11), National Institute of Standards and Technology (NIST), Gaithersburg, MD, 2023, http://dx.doi.org/10.18434/T4W30F, [Online]. Available: https://physics.nist.gov/PhysRefData/ASD/levels_form.html.

[26] P.D. Dumont, Y. Baudinet-Robinet, H.P. Garnir, E. Biemont, N. Grevesse, Phys. Rev. A 20 (1979) 1347–1351.

[27] D.C. Abbott, J. Phys. B 11 (1978) 3479, E. Biemont (private communication by Dumont et al [26]).

[28] M.A. Bautista, Astron. Astrophys. Suppl. Ser. 119 (1996) 105–110.

[29] S.N. Nahar, A.K. Pradhan, Phys. Scr. 61 (2000) 675–689.

[30] S.N. Nahar, F. Delahaye, A.K. Pradhan, C.J. Zeippen, Astron. Astrophys. Suppl. Ser. 144 (2000) 141.

[31] S.N. Nahar, M.A. Bautista, Astrophys. J. Suppl. 120 (1999) 327.

[32] B.C. Fawcett, At. Data Nucl. Data Tables 41 (1989) 181.

[33] K.M. Aggarwal, P. Bogdanovich, F.P. Keenan, R. Kisielius, At. Data Nucl. Data Tables 114 (2017) 1–60.

[34] K. Butler, C. Mendoza, C.J. Zeippen, (unpublished). The atomic data are available at the Opacity Project database TOPbase.

[35] G.X. Chen, A.K. Pradhan, J. Phys. B 32 (1999) 1809.

[36] C.X. Chen, A.K. Pradhan, Astron. Astrophys. Suppl. Ser. 136 (1999) 395.

[37] W. Eissner, M. Jones, H. Nussbaumer, Comput. Phys. Comm. 8 (1974) 270.

[38] R.H. Garstang, W.D. Robb, S.P. Rountree, Astrophys. J. 222 (3) (1978).

[39] H. Nussbaumer, P.J. Storey, Astron. Astrophys. 70 (1978) 37.

[40] W. Eissner, J. Phys. IV (Paris) C1 (1991) 3.

[41] S.N. Nahar, W. Eissner, G.X. Chen, A.K. Pradhan, Astron. Astrophys. 408 (2003) 789–801.

[42] A.K. Pradhan, S.N. Nahar, Atomic Astrophysics and Spectroscopy, Cambridge University Press, New York, 2011.

[43] S.N. Nahar, Astron. Astrophys. Suppl. Ser. 127 (2000) 253.

[44] S.N. Nahar, New Ast New 21 (2013) 8–16.

[45] S.N. Nahar, Astron. Astrophys. 448 (2006) 779.

[46] S.N. Nahar, Can. J. Phys. (2024) 1.

[47] S.N. Nahar, Atoms 12 (2024) 24.

[48] S.N. Nahar, A.K. Pradhan, JQSRT 155 (2015) 32–48.

[49] J.O. Ekberg, Phys. Scr. 12 (1975) 42.

[50] J.O. Ekberg, Phys. Scr. 11 (1975) 23.